Journal of Solid State Chemistry 184 (2011) 811–817

Contents lists available at ScienceDirect

Journal of Solid State Chemistry

journal homepage: www.elsevier.com/locate/jssc

Kinetic lattice Monte Carlo model for oxygen vacancy diffusion in praseodymium doped ceria: Applications to materials design

Pratik P. Dholabhai [a,*], Shahriar Anwar [a], James B. Adams [a], Peter Crozier [a], Renu Sharma [b]

[a] School for Engineering of Matter, Transport & Energy, Arizona State University, Tempe, AZ 85287, USA
[b] Center for Nanoscale Science and Technology, National Institute of Standards and Technology, 100 Bureau Drive, PO Box 6203, Gaithersburg, MD 20899, USA

ARTICLE INFO

Article history:
Received 14 October 2010
Received in revised form
1 February 2011
Accepted 6 February 2011
Available online 12 February 2011

Keywords:
Pr-doped ceria
Kinetic lattice Monte Carlo
Oxygen vacancy diffusion
Ionic conductivity
DFT+*U*

ABSTRACT

Kinetic lattice Monte Carlo (KLMC) model is developed for investigating oxygen vacancy diffusion in praseodymium-doped ceria. The current approach uses a database of activation energies for oxygen vacancy migration, calculated using first-principles, for various migration pathways in praseodymium-doped ceria. Since the first-principles calculations revealed significant vacancy–vacancy repulsion, we investigate the importance of that effect by conducting simulations with and without a repulsive interaction. Initially, as dopant concentrations increase, vacancy concentration and thus conductivity increases. However, at higher concentrations, vacancies interfere and repel one another, and dopants trap vacancies, creating a "traffic jam" that decreases conductivity, which is consistent with the experimental findings. The modeled effective activation energy for vacancy migration slightly increased with increasing dopant concentration in qualitative agreement with the experiment. The current methodology comprising a blend of first-principle calculations and KLMC model provides a very powerful fundamental tool for predicting the optimal dopant concentration in ceria related materials.

1. Introduction

Ceria related materials are considered to be one of the most promising materials for intermediate temperature fuel cell applications because of their high ionic conductivity, which in turn facilitates the reduction of their operating temperature and thereby eliminates several technological problems. As a result, oxygen vacancy migration in ceria and doped ceria has received major attention as it affects the performance of this material when used as the electrolyte and anode material within solid oxide fuel cells (SOFC) [1–6]. In our previous study, we highlighted various applications of praseodymium-doped ceria (PDC) [7] and presented a detailed first-principles (DFT+*U*) description of vacancy diffusion in PDC.

The results of those first principle calculations are ideally suited for input into kinetic lattice Monte Carlo (KLMC) models of vacancy diffusion. Monte Carlo methods have been used in the past to study materials for electrolyte applications in SOFC [8–13]. Most [8–10,12,13] of these studies used density functional theory (DFT) methodology and one [11] used semi-empirical potentials to determine the energetics for oxygen vacancy diffusion in oxides (yttria-stabilized zirconium and yttria-doped ceria). Among the studies performed using DFT methodology, some [8,9,12,13] of the studies determined activation energies from static calculations, and one [10] study determined energetics from *ab initio* molecular dynamics. The resulting activation energies were used as input into KLMC models of oxygen vacancy diffusion. However, none of these models included the effect of vacancy–vacancy interaction, which we find to be significant. Overall, these earlier calculations demonstrate that kinetic Monte Carlo is a powerful technique for investigating oxygen vacancy diffusion (and hence ionic conductivity) in doped oxides.

On the basis of percolation theory and neglecting the Coulomb repulsion between vacancies, Meyer et al. [14] deduced that for systems with fluorite structure, at low dopant concentrations, there are many percolating paths to enable vacancies to diffuse. They interpreted that at higher dopant concentration, many diffusion pathways are blocked due to attraction of vacancies to the dopants leading to a decrease in ionic conductivity. Previous calculations used Monte Carlo approaches to analyze oxygen mobility in complex oxide systems like CeO_2–ZrO_2 and CeO_2–ZrO_2–La_2O_3 in platinum catalysts [15], determining the equilibrium composition profile across a coherent interface in Sm-doped ceria [16]. Hull et al. [17] performed analysis of the total scattering using reverse Monte Carlo modeling of anion deficient ceria. They showed that the oxygen vacancies preferentially align

* Corresponding author.
E-mail addresses: pratik.dholabhai@asu.edu (P.P. Dholabhai), anwar@asu.edu (S. Anwar), jim.adams@asu.edu (J.B. Adams), crozier@asu.edu (P. Crozier), renu.sharma@nist.gov (R. Sharma).

0022-4596/$ - see front matter © 2011 Elsevier Inc. All rights reserved.
doi:10.1016/j.jssc.2011.02.004

as pairs in the (111) cubic directions as the degree of nonstoichiometry increases.

Molecular dynamics simulations have been used earlier to identify the trends in ionic conductivity as a function of dopant concentration. Hayashi et al. [18] used molecular dynamics simulations to investigate oxygen diffusion and the microscopic structure of ceria-based solid electrolytes with different dopant radii. Inaba et al. [19] studied oxygen diffusion in Gd-doped ceria using molecular dynamics simulations. They attributed the larger size of the trivalent Gd dopant ion to the higher calculated diffusion constant as compared to Y-doped ceria. An issue with molecular dynamics simulations is that they are performed over a very short time frame that can lead to insufficient statistical sampling of various configurations.

Since KLMC methods have proven very useful in the investigation of oxygen diffusion in other oxides, it makes sense to apply this methodology to Pr-doped ceria. Previous KLMC models have often suffered from two limitations: (1) very limited data on dopant effects on vacancy migration, often limited to a single binding energy, when in fact our calculations reveal that the dopant vacancy interactions can be very complex, and (2) a failure to include the effect of repulsion between the oxygen vacancies, which we will show is a significant effect at higher concentrations. In this article we develop a KLMC model that overcomes both of these limitations, and use it to investigate the effects of dopant concentration and temperature on ionic conductivity. Thus, the model can be used as a design tool to determine the optimal concentration of Pr dopants for maximizing ionic conductivity.

2. Computational methodology

Monte Carlo (MC) techniques were developed originally by Von Neumann, Ulam and Metropolis [20] and broadly refer to diverse approaches to unraveling problems involving the use of random numbers to sample the ensemble. Kinetic Lattice Monte Carlo (KLMC) is one such approach used to model lattice dynamics with the evolution of time. In the KLMC model, all atoms are assumed to occupy lattice sites that coincides with the local potential minimum with a potential barrier, E_{xy}, separating the adjacent lattice sites. The only meaningful events in KLMC simulations are those involving transfer or exchange of atoms from one lattice site to another. In this paper we focus on a vacancy diffusion mechanism, so we save computational memory and effort by only tracking the oxygen vacancies, and assume all other sites are occupied. In events where $E_{xy} \ll k_B T$, the transition rate of a vacancy moving from lattice site x to y is evaluated by the hopping mechanism governed by the Arrhenius Law:

$$q_{xy} = \upsilon_{xy} e^{(-E_{xy}/k_B T)} \tag{1}$$

Here, υ_{xy}, represents the attempt frequency for an atom hopping from lattice site x to y. The harmonic approximation of the effective attempt frequency corresponding to the defect vibrations can be expressed using the dynamical matrix theory [21] as:

$$\upsilon_{xy} = \frac{\prod_{i}^{3N} \upsilon_i^{min}}{\prod_{i}^{3N-1} \upsilon_i^{sad}} \tag{2}$$

where "υ^{min}" and "υ^{sad}" represent normal mode frequencies at the minimum and saddle point position of the hopping atom, respectively, and N is the numbers of ions. The KLMC model requires input rates for various allowable events, such as diffusion and reactions. One key aspect of the KLMC algorithm are these input rates, since if these rates are known then one can accurately simulate time-dependent diffusion of various species. The pros and cons of various approaches for identifying the rate process database in a KLMC simulation are explained by Adams et al. [22]. KLMC simulations based on a set of kinetic atomic-scale processes can describe the evolution of mesoscopic systems up to macroscopic times. In this way, we have developed a 3-D KLMC model of vacancy diffusion in ceria and doped ceria. This model will further enable us to calculate ionic conductivity of various doped materials with respect to the dopant concentration.

The KLMC technique is based on a blend of Monte Carlo's approaches and Poisson's processes. In the current KLMC model, the material in consideration can consist of various possible events and evolve as a series of independent events occurring in accordance with the input rates. Assuming Arrhenius's dependence, the diffusivity can be expressed as:

$$D = D_0 \exp\left(\frac{-\Delta E_A}{k_B T}\right) \tag{3}$$

where D_0 is the pre-exponential factor, T is the absolute temperature and k_B is the Boltzmann constant. The term ΔE_A generally comprises of two contributions: the total migration energy (ΔE_M), and the vacancy formation energy (ΔE_V). Primarily, most of the vacancies in ceria-related materials are generated to maintain the charge balance due to the addition of aliovalent dopants. For example, the addition of Pr^{+3} to CeO_2 results in an oxygen vacancy for every two ionized dopants (this is the stoichiometric vacancy to dopant ratio of 0.5). Moreover, the vacancy formation energy in ceria and doped ceria is very high; hence, the concentration of vacancies created thermally in the electrolyte is extremely small. Consequently, the vacancy formation energy (ΔE_V) term can be neglected and effectively the energy term in Eq. (3) consists only of vacancy migration energy (ΔE_M). We have argued earlier [7] that the activation energy for vacancy migration is actually a complex average of many jump events. In this regard, we have calculated many activation energies of various diffusion pathways for oxygen vacancy migration in PDC for a vacancy hopping mechanism [7]. The energies from our previous work [7], as presented in Table 1, are input to the KLMC model. It should be noted that, for PDC, the oxygen prefers a second nearest neighbor (2NN) site, which means that many types of jump events need to be included (1NN→2NN, 2NN→2NN, 2NN→3NN, etc.) to properly model the complexity.

The average rate of displacement of defects in solids by thermal activation can be calculated using classical rate theory [23]. Accordingly, the hopping rate for the defect can be expressed by Eq. (1). The pre-exponential factor (D_0) in Eq. (3) mainly consists of the jump distance (for ceria it is half the length of the lattice parameter) and the hopping rate for the migrating vacancy. In the current work, the jump distances for all first

Table 1
Activation energies for oxygen vacancy migration along distinctive pathways in PDC calculated using first-principles. $E_{x,y}$ denotes activation energy for an oxygen atom migrating from X-nearest neighbor (XNN) to Y-nearest neighbor (YNN) with respect to the Pr ion in PDC.

Migration pathway	Activation energy (eV)
$E_{(1,1)}$	0.78
$E_{(1,2)}$	0.41
$E_{(1,3)}$	2.79
$E_{(2,1)}$	0.43
$E_{(2,2)}$	0.47
$E_{(2,3)}$	0.57
$E_{(3,1)}$	2.69
$E_{(3,2)}$	0.44
$E_{(3,3)}$	0.47

neighbor jumps were assumed to be constant for various dopant concentrations as very small changes in O–O bond length ($\sim$0.001 nm) are expected. The attempt frequency (5×10^{12} Hz) was determined from Eq. (2). It is the ratio of the product of $3N$ normal frequencies of the entire system at the starting point of the transition to the $3N$—1 frequencies of the system constrained in the saddle point configuration This value of attempt frequency was assumed constant for different configurations, as the normal mode frequencies are not expected to differ significantly.

The KLMC model comprises of a number of ordered events which take place in a sequence as given in the flowchart in Fig. 1. We computed the mean square displacement of all the vacancies in the simulation cell (accounting for crossing periodic boundaries) and used the results to calculate the diffusion coefficient of oxygen vacancies as follows:

$$D_v = \lim_{t\to\infty} \sum_{i=1}^{N} \frac{|R_i(t) - R_i(0)|^2}{6t} \tag{4}$$

where t is the sum of all the time steps Δt, for each jump event and $R_i(t)$ is the position of the ith vacancy at time t. Following the computation of oxygen vacancy diffusion coefficient, the ionic conductivity was calculated using the Nernst–Einstein relation as given below [1]:

$$\sigma_i = \frac{D_v C_i (qe)^2}{k_B T} \tag{5}$$

where σ_i is the ionic conductivity, C_i is the concentration of ionic carriers (vacancies for the present case) and qe their charge.

We used a $10 \times 10 \times 10$ cell comprising of 12,000 possible sites to place the respective ion. The periodic cell with a $10 \times 10 \times 10$ periodicity was built from a conventional 12-atom cubic unit cell of ceria using the theoretically optimized lattice constant of 0.5494 nm for bulk ceria [7]. Of these 12,000 positions, 4000 are available for dopant placement and 8000 sites for vacancy formation. The vacancies are allowed to hop to adjacent sites, subject to certain constraints. The simulation cell was repeated periodically along the three axes to simulate a lattice of effectively infinite extent. The dopant and vacancy concentrations were varied. All the dopant ions are assumed to be trivalent; hence, for every two dopant ions, a vacancy was incorporated. For each of the different dopant concentrations, ten simulations were performed, each with a different dopant distribution. Each simulation comprised of approximately 3000,000 or more jump events. This resulted in achieving a statistical average with a precision of $\approx$3% for various dopant concentrations. Considering the difference of the order of $\approx$3% in ionic conductivity for the simulations involved, the sampling does not require additional runs for each configuration. The simulations were performed for temperatures ranging from 673 to 1073 K and approximately equal diffusion distances were used to calculate the final diffusion coefficients. To plot the Arrhenius relationship and facilitate comparison with the available experimental data, some specific configurations were simulated for temperature ranging from 573 to 1173 K.

We have developed two separate models for PDC, a Vacancy Non-Repelling model (VNR) and a Vacancy Repelling model (VR). We performed preliminary calculations using the DFT+U methodology explained in our previous work [7] to investigate vacancy diffusion in PDC. All the calculations were performed for charge neutral supercells. We studied two separate cases for PDC: (i) vacancies are placed next to the dopant ions and (ii) vacancies are placed far apart from the dopant ions. For case (i), we found that the configuration involving two vacancies separated by a distance larger than the 1NN (nearest-neighbor) distance is more stable by 0.38 eV as compared to the configuration with vacancies placed next to each other. For case (ii), the configuration involving two separated vacancies is more stable by 0.28 eV as compared to the configuration with vacancies placed next to each other. The observed Coulomb interaction between charged vacancies lead us

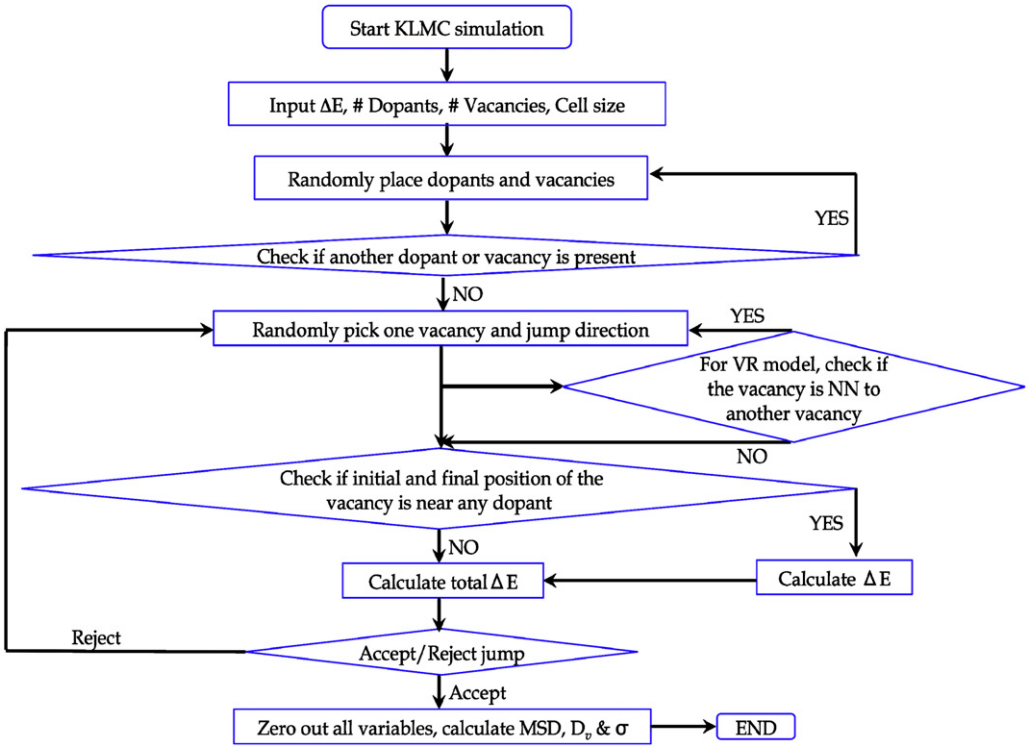

Fig. 1. Flowchart of the major events involved in a KLMC simulation. NN and MSD represent the next neighbor and mean square displacement, respectively; D_v is the diffusion coefficient and σ is the conductivity.

to develop two separate models: (1) in the VNR model, vacancies are allowed to move anywhere in the simulation cell except into an existing vacancy and (2) in the VR model, the vacancies are not allowed to move adjacent (first nearest neighbor) to any other vacancies in the simulation cell, nor into an existing vacancy. (It would be slightly more accurate to add the repulsion energy. But the repulsion energy is so large that it is very rare that vacancies will move adjacent to one another, so this is a very good approximation). Previous studies have neglected the Coulomb interaction between the anionic species, but we find that this effect is important in correctly characterizing the optimal dopant concentration in ceria related electrolyte materials.

3. Results and discussion

The energies given in Table 1 correspond to vacancy motion adjacent to one trivalent Pr ion as shown in Fig. 2. In the presence of multiple dopant ions, we use an underlying assumption that every additional Pr dopant in the vicinity of the migrating vacancy will have an additive effect towards the activation energy for vacancy migration. For example, for paths (Table 1), 1NN→2NN and 2NN→1NN, we found that the decrease in activation energy for ceria doped with two Pr ions located next to each other was twice as much compared to ceria doped with two Pr ions that are separated. Using first principles calculations [7] we found that in vicinity of two next neighbor Pr dopant ions, the decrease in activation energy relative to the undoped ceria for the migration path 1NN→2NN is 0.13 eV as compared to 0.06 eV in presence of one Pr dopant ion. Similarly, for the migration path 2NN→1NN, the respective numbers are 0.07 and 0.04 eV. In the KLMC model, for the migration paths 1NN→2NN and 2NN→1NN in presence of two Pr dopant ions, the decrease in activation energy is calculated to be 0.12 and 0.08 eV, respectively. These numbers justify the assumption (additive effect of dopants) incorporated in the KLMC model and provide a reasonable approximation of migration energies in the presence of multiple dopants. Moreover, this decrease in activation energy for the case where two Pr ions are next to each other is in reasonably good agreement with results reported by Andersson et al. [24]. Using this relationship in the KLMC model, we have simulated diffusion of oxygen vacancies in the presence of multiple dopants. Under the current assumption, the estimated activation energies for multiple dopants are probably valid to about 10 meV at low to moderate concentrations, but may be larger at higher concentrations.

One of the principal goals of the current effort is to study the variations in ionic conductivity as a function of dopant concentration in PDC and to determine the optimal dopant concentration that exhibits a maximum in ionic conductivity. As mentioned earlier, researchers have previously studied other systems with similar methodology, but have neglected the Coulomb interactions between the charged vacancies. Hence, we also wish to investigate the significance of including these effects. Fig. 3(a) comprises the simulation results for variations in ionic conductivity as a function of dopant concentration in PDC using the KLMC–VNR model for temperatures ranging from 673 to 1073 K. For the temperatures ranging from 673 to 873 K, the maximum in ionic conductivity is observed at ≈25% dopant concentration, whereas the maxima at temperatures of 973–1073 K are shifted

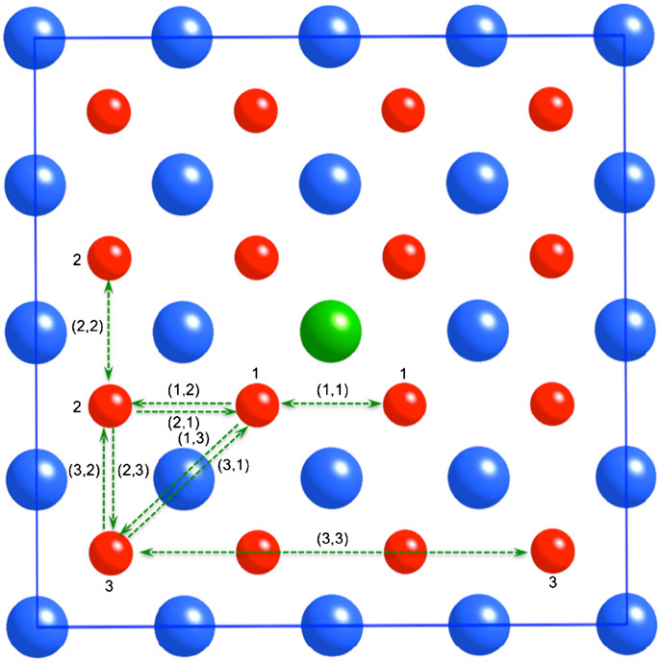

Fig. 2. Top view of a $2\times2\times2$ PDC supercell. The blue, green and red balls represent Ce, Pr and O ions, respectively. Numbers 1, 2 and 3 represent 1NN, 2NN and 3NN oxygen ions with respect to the Pr ion, respectively. (X, Y) represents an oxygen ion jump from XNN to YNN. Pr ion closer to the migrating vacancy is only shown. (For interpretation of the references to colour in this figure legend, the reader is referred to the web version of this article.)

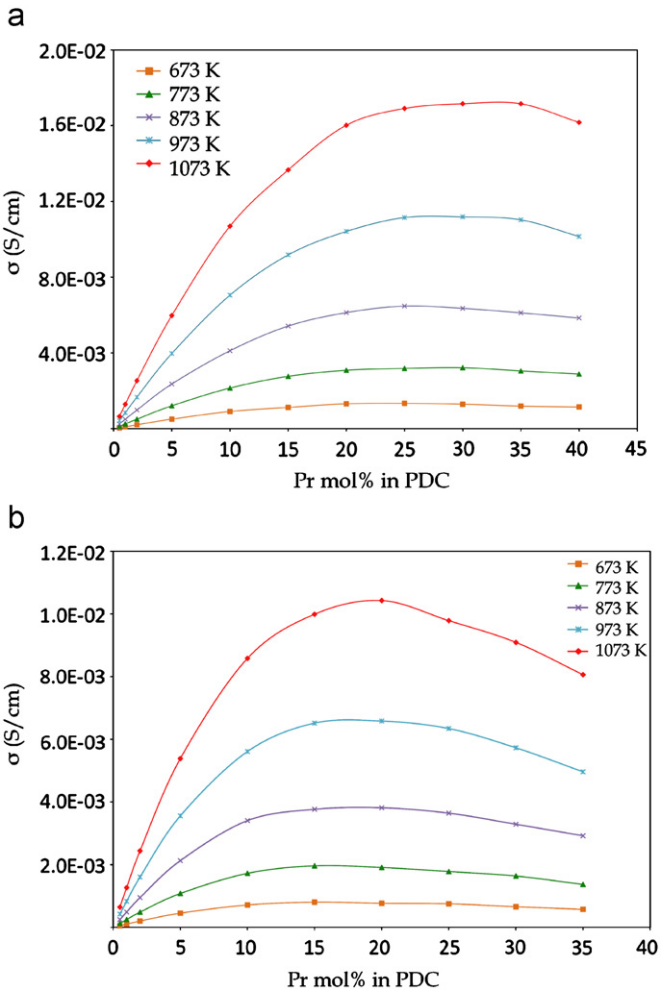

Fig. 3. (a) Plot of calculated ionic conductivity of PDC as a function of dopant concentration generated using KLMC-VNR model for temperature ranging from 673 to 1073 K. (b) Plot of calculated ionic conductivity of PDC as a function of dopant concentration generated using KLMC-VR model for temperature ranging from 673 to 1073 K.

at ≈30% dopant concentration. Incorporating the effects of charged vacancies using the VR model significantly changes the results. Plotted in Fig. 3(b) are the variations in ionic conductivity as a function of dopant concentration in PDC using the KLMC–VR model for temperatures ranging from 673 to 1073 K. The overall effect of the VR model is to reduce vacancy diffusion, especially at higher concentrations, which also results in a shift of the peak conductivity towards lower concentrations. For the temperatures of 673–773 K, the maximum in ionic conductivity is predicted at ≈15% dopant concentration, whereas the maximum at temperature ranging from 873 to 1073 K is predicted at ≈20% dopant concentration.

Considering all the simulations performed for PDC using KLMC–VNR and VR models, the magnitude of ionic conductivity is larger for the values obtained using the VNR model. This is a consequence of the fewer number of available sites for the vacancies to migrate on the oxygen sublattice for the VR model due to the vacancy-repelling factor, which decreases the diffusion coefficient. The computed maximum in ionic conductivity at around 25–30% dopant concentration using the KLMC–VNR model agrees well with experiment [25,27], but does not provide the true picture. Praseodymium is known to have mixed valence at atmospheric pressure; hence, equilibrium between Pr^{4+} and Pr^{3+} exists is determined by the temperature and oxygen pressure. Hence, only half of the dopant ions are Pr^{3+} [25,28]. This equilibrium reduces the probable oxygen vacancy concentration upon doping with Pr; hence, the ionic conductivity increases more slowly with increase in Pr content as compared to other aliovalent dopants [29]. In the current simulations performed using both VNR and VR models, all the Pr dopant ions are assumed to be trivalent. Hence, the results obtained with the KLMC models should be compared with experimental data plotted vs. ionized dopants, not total dopants. In some cases it has been estimated that only half of the dopants are ionized, so this is a large effect.

Experimental studies by Shuk and Greenblatt [25] and Chen et al. [27] found that the maximum in ionic conductivity occurred at about 30% dopant concentration. If we assume that approximately half of these dopants are trivalent (in the experiment, only half of the dopants are ionized) [25,27], the optimal concentration of dopants (≈15–20%) as predicted by the KLMC–VR model is in reasonably good agreement with the measured values. Moreover, the slight discrepancy in the experimental and theoretical findings can be attributed to the dependence of oxygen vacancy concentration on the temperature and oxygen partial pressure, and also to grain boundary effects, effects that are not included in the KLMC model.

To further investigate the origin behind the calculated maximum in the ionic conductivity, we performed additional simulations using the KLMC–VR model at 873 K. Fig. 4 shows two different scenarios: (i) the vacancy concentration is increased linearly keeping the dopant concentration fixed at 20% and (ii) increasing the dopant concentration linearly and keeping the vacancy concentration fixed at 5%. For case (i), the ionic conductivity keeps increasing, as shown in the figure. The slight dip in the curve is due to vacancy–vacancy interactions at higher vacancy concentration, but this effect is modest. Case (ii) results in a steadily decreasing ionic conductivity. The conductivity decreases in case (ii) because a growing fraction of the vacancies get trapped near the dopant ions, decreasing the net diffusion. This effect is significantly larger than the effect of vacancy–vacancy interactions (case (i)), which also decreases ionic conductivity.

Overall, these two investigations explain the increase and then decrease in ionic conductivity with increasing dopant concentration. Initially, the ionic conductivity increases at lower dopant concentration due to the increase in vacancy concentration, but after reaching a maximum, it decreases due to increasing interactions between the dopant ions and vacancies that serves as a bottleneck, decreasing the number of minimum energy pathways for a vacancy to diffuse.

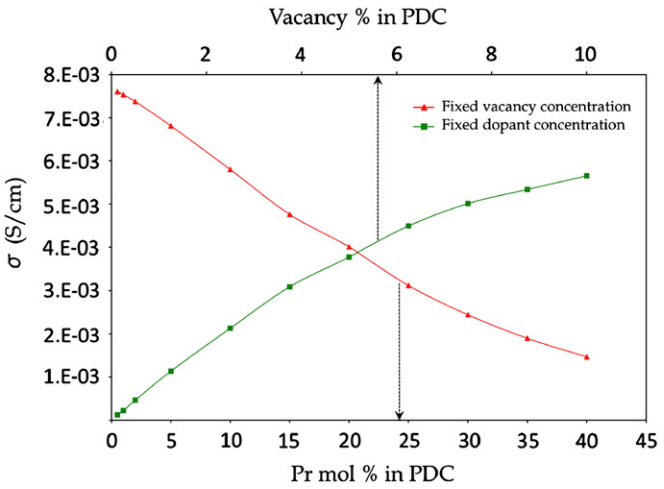

Fig. 4. Plot of calculated ionic conductivity as a function of fixed dopant concentration and fixed vacancy concentration using the KLMC-VR model at 873 K. For the plot with fixed dopant concentration, the *x*-axis represents the varying vacancy concentration.

Nauer et al. [26] reported that the total conductivity of PDC increases until a dopant concentration of 40–50% is reached. This is due to the fact that for PDC, beyond 25–30% dopant concentration, the electronic conductivity exceeds the ionic conductivity [25]; hence, explains the higher dopant concentration for attaining a maximum in electrical conductivity. Fig. 5(a) shows the plot of ionic conductivity versus dopant concentration at 973 K using the KLMC–VNR and VR model. Fig. 5(b) shows data obtained by experimental measurements performed by Shuk and Greenblatt [25] and Chen et al. [27]. Depending on the fraction of dopants that are trivalent, the graph obtained using the KLMC–VR simulations should be shifted somewhat towards the right. This is in reasonable agreement with experimental data if the vacancy concentration is half (in the experiment, only half of the dopants are ionized) of what should be expected after the addition of Pr dopant [25,27]. The primary reason for the discrepancy in the absolute magnitude of the conductivity as observed from the experimental measurements, as shown in Fig. 5(b), is probably due to the difference in synthesis methods of the respective samples [25,27]. Overall, Fig. 5 shows that the trend of increased conductivity in PDC can be reasonably predicted using KLMC–VR model if the fraction of ionized dopants is known.

The primary reason for the decrease in the ionic conductivity with increasing dopant concentration is the increase in average activation energy for vacancy migration and the percent increase of Pr ions near the migrating vacancy. The increasing number of Pr ions often tends to bind the neighboring oxygen vacancy more strongly and decrease the diffusion coefficient, which in turn decreases the oxide ion conductivity. At low dopant concentration, the number of available minimum energy diffusion pathways is higher. For PDC, the formation of an oxygen vacancy is found to be most favorable at the 2NN position [7] to the Pr dopant; hence, the available minimum energy pathways keep decreasing with increasing of dopant ion concentration leading to this behavior. Thus the simulations results, obtained using the KLMC–VR model, show reasonable agreement with the experimental data and highlight the importance of including the

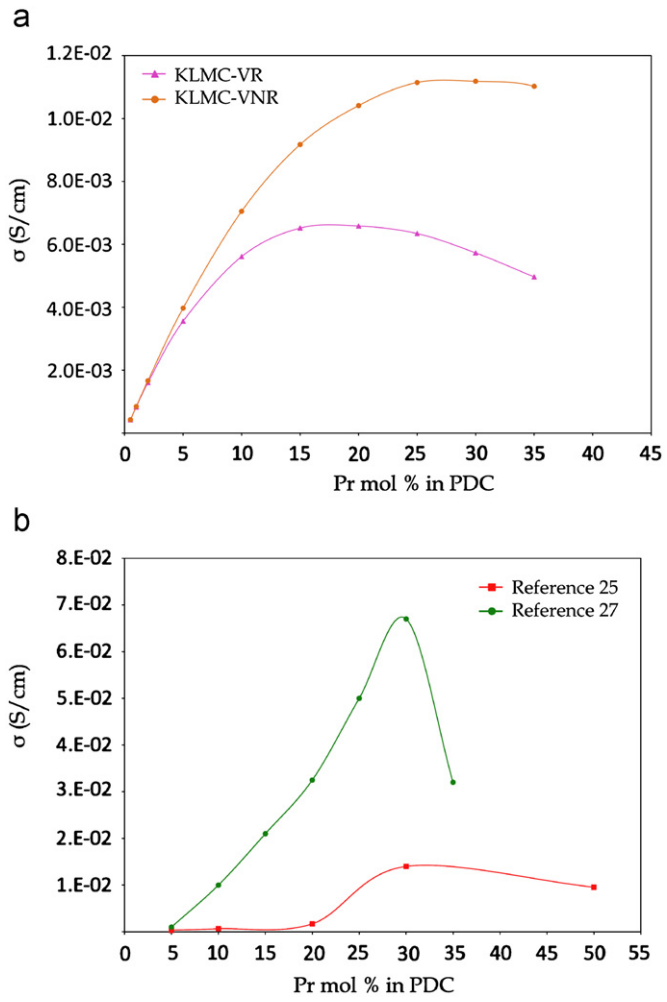

Fig. 5. (a) Ionic conductivity data calculated for PDC obtained using KLMC-VNR and VR models for simulations performed at 973 K. In both KLMC models, we assume that all the dopants are ionized. (b) Ionic conductivity data for PDC obtained by experimental measurements performed at 973 K. For the experimental results from Refs. [25,27], only half of the dopants are ionized.

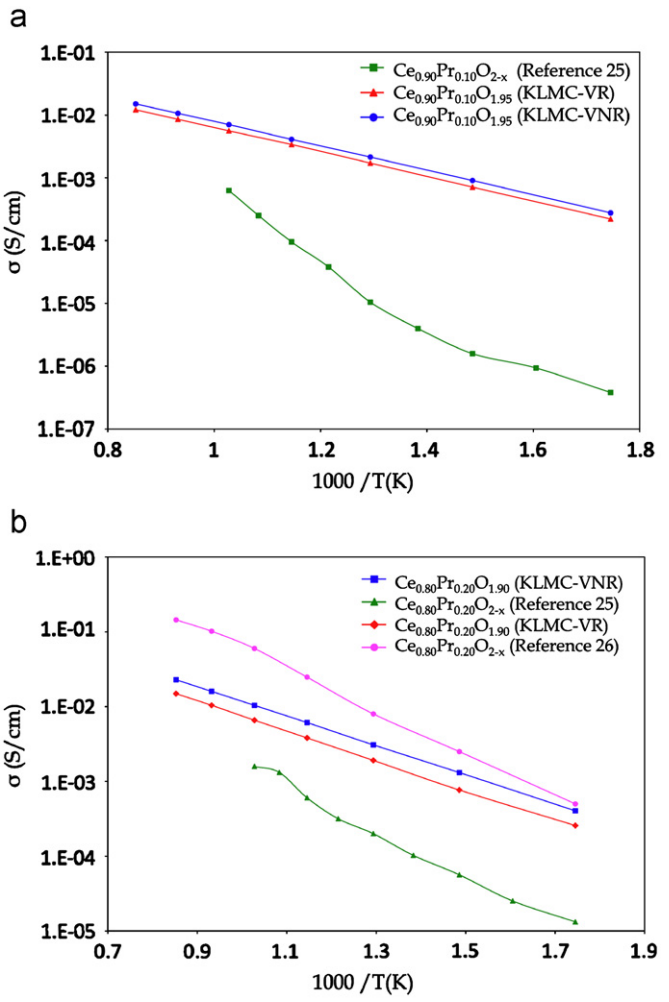

Fig. 6. (a) Arrhenius plot of ionic conductivity of 10 mol% PDC as a function of temperature ranging from 573 to 1173 K for the KLMC simulations and 573 to 973 K for the data measured by experiments. (b) Arrhenius plot of ionic conductivity of 20 mol% PDC as a function of temperature ranging from 573 to 1173 K for the KLMC simulations and 573 to 973 K for the data measured by experiments.

Coulomb interactions between the anionic species. Hence, the current methodology serves as a fundamental tool for predicting the optimal dopant concentration in PDC.

Fig. 6(a) and (b) shows values of ionic conductivity as a function of inverse temperature for $Ce_{0.90}Pr_{0.10}O_{2-x}$ and $Ce_{0.80}Pr_{0.20}O_{2-x}$, respectively, obtained from KLMC simulations and experimentally measured values [25,26]. The Arrhenius type behavior of the ionic conductivity for this particular configuration is visible with all the simulation data points for KLMC–VNR and VR models lying on straight lines. The simulation results agree reasonably well with the experiments with some discrepancy in the magnitude of ionic conductivity, but this could be due to the reasons mentioned above. For Fig. 6(b), our theoretical results are in the middle of two sets of experimental measurements, and the trends with temperature are very similar. Ref. [26] is the total conductivity, whereas our model and Ref. [25] included only the ionic contribution to the conductivity. Several other plots for different compositions have been studied and the general trends and conclusions that can be drawn are analogous.

A vacancy can move through a number of distinctive diffusion pathways before finally diffusing across an ionic conductor such as PDC. Determination of the rate-limiting step for a path is complex, because it depends on the dopant concentration and arrangement. The input rates used for the KLMC simulations were evaluated using the DFT+U calculations [7] and provide a very reasonable initial assumption, but the migration energy for a complete diffusion path cannot be associated with a single migration event. It has to be averaged using a statistical model that takes into account the distinct pathways involved during diffusion. Moreover, the migration energies generated using first-principles are applicable for processes occurring at 0 K. Hence we have compared the statistically averaged migration energies elucidating the temperature dependence with the experimentally measured values. Fig. 7 shows averaged activation energy for vacancy migration as a function of dopant concentrations. The activation energies presented in Fig. 7 are computed from the slopes of similar Arrhenius plots as seen in Fig. 6(a) and (b).

The plots of average activation energy as a function of dopant concentration generated using KLMC–VNR and KLMC–VR simulations show similar behavior with the former having slightly lower magnitude. The experimental values taken from the measurements performed by Shuk and Greenblatt [25] are compared with those obtained from simulations in Fig. 7. The experimental and theoretical values are in good agreement at low dopant concentrations, and both increase with increasing dopant concentration, but the effect is larger for the experimental data, although there are significant error bars. The small increase in the activation

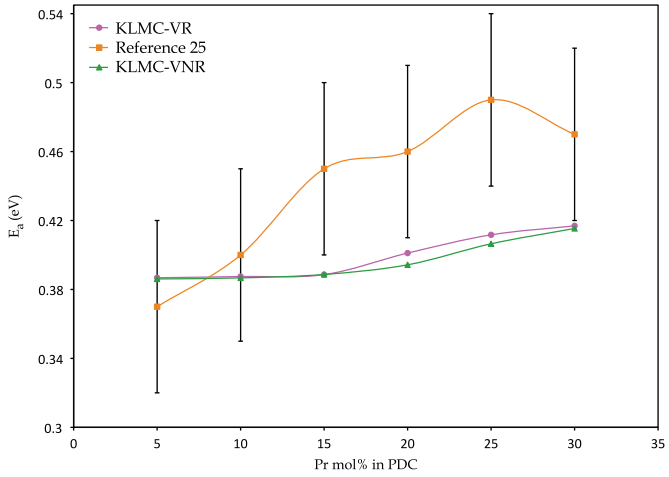

Fig. 7. Average activation energy as a function of dopant concentration for PDC compared with the available experimental data. The experimental data involves error bars of 50 meV.

energy for vacancy migration at dopant concentrations ranging from 5 to 15% as seen in Fig. 7 from simulations is primarily due to negligible interactions between oxygen vacancies and dopant ions. At higher dopant concentrations, the increase in average activation energy for migration is due to the increased likelihood of finding two next neighbors Pr–Pr or Pr–Ce ions pairs near an oxygen vacancy, where a higher energy is needed to overcome these barriers. Any further increase in the Pr ions can eventually trap the vacancy and form a bottleneck for diffusion. This is also evident from the earlier explanation and Fig. 4, where the increase in dopant concentration is found to be primarily responsible for the decrease in ionic conductivity after attaining a maximum. The differences between theory and experiment may be partly due to: (1) limitations in the DFT data used as input, (2) assumptions involved in the KLMC model regarding activation energies, (3) the uncertainty of the order of 50 meV in measured values, (4) the experimental samples are polycrystalline, so grain boundaries may have a small effect and (5) variations in sintering temperature may affect the level of reduction of the experimental samples. Nauer et al. [26] reported an experimentally measured value of activation energy ranging between 0.42 and 0.53 eV for 20% dopant concentration for PDC as compared to the average activation energy value 0.39 eV obtained for similar dopant concentration by KLMC simulations. Keeping this in mind, the averaged activation energies obtained from KLMC simulations are in reasonable agreement with the measured values.

4. Conclusions

We have used KLMC simulations in conjunction with our previously performed first-principles calculations to investigate oxygen vacancy diffusion in PDC. The increase in average activation energy for vacancy migration as a function of dopant concentration is due to the increase in Pr–Pr dopant pairs that hinder further motion of the oxygen vacancies. The current findings are found to follow similar trends as compared with the previously measured values. A dopant concentration of approximately 15–20% is found to be optimal for achieving maximum ionic conductivity in PDC. The KLMC simulations are in reasonably good agreement with the available experimental data, when we take into account that only about half of the dopants are ionized. The decrease in ionic conductivity with increasing dopant concentration is correlated with the increase in average activation energy for vacancy migration from the vicinity of the dopant pairs and the subsequent decrease in availability of minimum energy pathways for the vacancy diffusion. Based on the reasonable agreement with experimental measurements, we believe that the current model can be used as a design tool to predict the optimal dopant concentration for attaining maximum ionic conductivity.

The KLMC code developed for this project will be available for download in the near future from: http://enpub.fulton.asu.edu/cms/

Acknowledgments

This paper is based on the work supported by the Department of Energy under the Grant no. DE-PS02-06ER06-17. The authors gratefully acknowledge the Fulton High Performance Computing Initiative (HPCI) at the Arizona State University for the computational resources.

References

[1] A. Trovarelli, Catalytic Science Series 2, Catalysis by Ceria and Related Materials, 15, 2002.
[2] S. Sharma, S. Hilaire, J.M. Vohs, R.J. Gorte, H.W. Jen, J. Catal. 190 (2000) 199.
[3] H.L. Tuller, J. Phys. Chem. Solids 55 (1994) 1393.
[4] H. Inaba, H. Tagawa, Solid State Ionics 83 (1996) 1.
[5] M. Mogensen, N.M. Sammes, G.A. Tompsett, Solid State Ionics 129 (2000) 63.
[6] B.C.H. Steele, A. Heinzel, Nature 404 (2001) 345.
[7] P.P. Dholabhai, J.B. Adams, P. Crozier, R. Sharma, J. Chem. Phys. 132 (2010) 094104.
[8] R. Pornprasertsuk, P. Ramanarayanan, C.B. Musgrave, F.B. Prinz, J. Appl. Phys. 98 (2005) 103513.
[9] R. Pornprasertsuk, T. Holme, F.B. Prinz, J Electron. Soc. 156 (2009) B1406.
[10] R. Krishnamurthy, Y.G. Yoon, D.J. Srolovitz, R. Car, J. Am. Ceram. Soc. 87 (2004) 1821.
[11] A.D. Murray, G.E. Murch, C.R.A. Catlow, Solid State Ionics 18 (1986) 196.
[12] S.B. Adler, J.W. Smith, J.A. Reimer, J. Chem. Phys. 98 (1993) 7613.
[13] S.B. Adler, J.W. Smith, J. Chem., Soc. Farad. Trans. 89 (1993) 3123.
[14] M. Meyer, N. Nicoloso, V. Jaenisch, Phys. Rev. B 56 (1997) 5961.
[15] D. Efremov, L. Pinaeva, V. Sadykov, C. Mirodatos, Solid State Ionics 179 (2008) 847.
[16] A. Walle, D.E. Ellis, Phys. Rev. Lett. 98 (2007) 266101.
[17] S. Hull, S.T. Norberg, I. Ahmed, S.G. Eriksson, D. Marrocchelli, P.A. Madden, J. Solid State Chem. 182 (2009) 2815.
[18] H. Hayashi, R. Sagawa, H. Inaba, K. Kawamura, Solid State Ionics 131 (2000) 281.
[19] H. Inaba, R. Sagawa, H. Hayashi, K. Kawamura, Solid State Ionics 122 (1999) 95.
[20] N. Metropolis, S. Ulam, J. Am. Stat. Assoc 44 (1949) 335.
[21] F. El-Mellouhi, N. Mousseau, P. Ordejon, Phys. Rev. B 70 (2004) 205202.
[22] J.B. Adams, Z. Wang, Y. Lia, Thin Solid Films 365 (2000) 201.
[23] G.H. Vineyard, J. Phys. Chem. Solids 3 (1957) 121.
[24] D.A. Andersson, S.I. Simak, N.V. Skorodumova, I.A. Abrikosov, B. Johansson, Proc. Natl. Acad. Sci. USA 103 (2006) 3518.
[25] P. Shuk, M. Greenblatt, Solid State Ionics 116 (1999) 217.
[26] M. Nauer, Ch. Fticos, B.C.H. Steele, J. Eur. Ceram. Soc. 14 (1994) 493.
[27] M.J. Chen, S. Cheng, F.Y. Wang, J.F. Lee, Y.L. Tai, Electron. Soc. Trans **7** (2007) 2245.
[28] H. Inaba, K. Naito, J. Solid State Chem. 50 (1983) 100.
[29] W. Huang, P. Shuk, M. Greenblatt, Chem. Mater. 9 (1997) 2240.